PCCP

Accepted Manuscript

This is an *Accepted Manuscript*, which has been through the Royal Society of Chemistry peer review process and has been accepted for publication.

Accepted Manuscripts are published online shortly after acceptance, before technical editing, formatting and proof reading. Using this free service, authors can make their results available to the community, in citable form, before we publish the edited article. We will replace this *Accepted Manuscript* with the edited and formatted *Advance Article* as soon as it is available.

You can find more information about *Accepted Manuscripts* in the Information for Authors.

ROYAL SOCIETY OF CHEMISTRY

www.rsc.org/pccp

Stable and Efficient Carbazole-Based Amphiphilic Ru (II) Sensitizers for Dye-Sensitized Solar Cells

Hammad Cheema[a], Robert Younts[b], Bhoj Gautam[b], Idriss Bedja[d], Ravindra Kumar Gupta[d],

Ashraful Islam[c], Liyuan Han[c], Kenan Gundogdu[b], Ahmed El-Shafei*[a]

[a]*Polymer and Color Chemistry Program, North Carolina State University, Raleigh, NC, 27695, USA*

[b]*Physics Department, North Carolina State University, Raleigh, NC, 27695, USA*

[c]*Photovoltaic Materials Unit, National Institute for Materials Science, 1-2-1 Sengen, Tsukuba, Ibaraki 305-0047, Japan*

[d]*CRC, Optometry Department, College of Applied Medical Sciences, King Saud University, Riyadh 11433, Saudi Arabia*

ABSTRACT

Here we report two novel amphiphilic Ru (II) heteroleptic bipyridyl complexes HD-14 and HD-15, compared to previously reported NCSU-10. We have combined the strong electron donor characteristics of carbazole and hydrophobic nature of different long alkyl chains, C7, C18 and C2 (NCSU-10), tethered to N-carbazole to study their influence on photocurrent, photovoltage and long term stability for dye-sensitized solar cells. Photon harvesting efficiency and electron donating characteristic of carbazole-based ancillary ligands were found to be unaffected by

different alkyl chain lengths. However, slight drop in the V_{oc} of HD-14 and HD-15 was observed compared to that of NCSU-10. It was found by nanosecond flash photolysis transient absorption (TA) measurements that the faster the dye regeneration the higher the photocurrent density response will be and the dye regeneration time was found to be 2.6, 3.6, and 3.7 μs for HD-14, HD-15, and N719 dyes, respectively. The difference in the amplitude of transient absorption (TA) signal of the oxidized dye as measured by femtosecond TA studies is in excellent agreement with the photocurrent generated, which was in the following order HD-14>HD-15>N719. Under 1000 h light soaking conditions, HD-15 maintained up to 98% (only 2% loss) of initial power conversion efficiency compared to 8% loss for HD-14 and 22% loss in power conversion efficiency for NCSU-10. HD-15 was strikingly stable to light soaking conditions when employed in the presence of ionic liquid electrolyte, which paves the way for wide spread applications of dye-sensitized solar cells with long term stability. The total power conversion efficiency (η) was 9.27% for HD-14 and 9.17 % for HD-15 compared to 8.92% of N719.

1. INTRODUCTION

It is unfortunate that until today, most of the current energy demands are met by fossil fuels. To realize the dream of low carbon society, and ensure the wide spread application of renewable energy sources such as solar energy, photovoltaic devices should be highly efficient, cheap and stable for longer time. Solar energy has been recognized as one of the cleanest, most reliable and abundantly available renewable energy sources on the planet Earth[1]. Compared to silicon-based single layer p-n junction photovoltaic, dye-sensitized solar cells (DSCs) are a promising candidate for alternative form of solar cells owning to their unique features of being flexible and efficient in year around conditions[2-5]. Since the breakthrough report by O'Regan and Grätzel[6], immense research has been carried out to better understand, and improve the fundamental

science of this technology. As a result, DSCs with efficiency as high as 13 % *(η)* [7] was achieved by Zn-porphyrin complex. Additionally, perovskite-sensitized solid state dye solar cells have reached record high efficiency of 15.9% [8], and efficiencies of 17.9% [9] and 19.3% [10]were reported recently. However, perovskite solar cells contain Pb and are far behind in long term stability compared to DSCs[10].

Owing to unique nature of DSC's where electron injection, charge transport, and hole carrier is achieved by different components, achieving higher efficiency is dependent on the optimization of the components of the device including a dye (sensitizer), TiO_2 and electrolyte. Sensitizer is one of the most critical components within a DSC; it determines not only the light harvesting efficiency, but also mediates the interaction between redox shuttle and TiO_2 [11, 12]. Thus the chemical nature of the sensitizer not only determines the operational efficiency of DSC but also sets the standards for long term stability as reported for Ru (II) sensitizers Z-907[13] (Fig. 1).,. Z-907 showed strikingly good long term stability owing to long alkyl chains and polymer gel electrolyte as redox shuttle. Z-907 resulted in slightly less (6%) power conversion efficiency owing to lack of any electron donor groups. The lack in efficiency of Z-907 was circumvented by the introduction of electron rich groups such as thiophene for C-103[14] and C-104[15]. Several groups have reported Ru (II) sensitizers based on carbazole such as CYC-B6L and CYC-B6S[16], JK-142[17], CYC-B13[18] (Fig. 1), which showed promising efficiency and long term stability. However, the carbazole-based bipyridyl ancillary ligands used were complex and synthesized using multistep synthetic routes.

Figure 1. Molecular structures of complexes Z-907, JK-142 and CYC-B13.

Recently, our group reported a much simple yet highly efficient sensitizer NCSU-10 [19] based on carbazole bipyridyl ancillary ligand. The corresponding bipyridyl ancillary ligand was synthesized by one step Knoevenagel type condensation reaction[19-22]. Sensitizer employing that ancillary ligand was coded as NCSU-10 and is shown in Figure 2. Thus carbazole ancillary ligands and long alkyl chains are well known precursors for designing high efficiency Ru (II) sensitizers. However, there are no studies which have reported the effect of long alkyl chains tethered directly to the nitrogen of carbazole on the photophysical, photovoltaic and long term stability properties of Ru (II) sensitizers.

In this study, we have reported a systematic study of combining the strong electron donor characteristic of carbazole and charge recombination suppressing properties of different alkyl chain lengths and their effect on long term stability of DSC's. The main objective was to design sensitizers which are simple to synthesize, highly efficient and show unprecedented long term stability. Impedance spectroscopy was employed to investigate the photophysics and charges at the interface of the proposed sensitizers while anchored to TiO_2. Photovoltaic characterization (I-V curve and IPCE) were carried out on solar cells with and without TBP (tert-butylpyridine) and DCA (deoxycholic acid) as additives to determine the best working conditions for HD-14

and HD-15. The decay of transient absorption (TA) signal in nanosecond laser flash photolysis experiment is correlated to dye regeneration, whereas dynamics of TA signal for oxidized dye in femtosecond TA studies is associated with electron injection dynamics. The strategy of tethering long alkyl chain to N-carbazole resulted in highly efficient sensitizers which outperformed the benchmark N719 in photocurrent density (J_{sc}), power conversion efficiency and long term stability. Comparison of the effect of different alkyl chain lengths of C7 (HD-14) and C18 (HD-15) on photocurrent, photophysics, interface properties with TiO_2 and long term stability was carried out, and HD-15 was found to be strikingly stable to light soaking conditions when employed in presence of ionic liquid electrolyte.

2. RESULTS AND DISCUSSION

For the synthesis of proposed sensitizers HD-14 and HD-15, the corresponding N-substituted carbazoles were first synthesized according to procedure given in literature[23]. Then, the formylation reaction of respective N-substituted carbazole was carried out under Vilsmeier-Hack reaction conditions[24], which resulted in 9-heptyl-9H-carbazole-3-carbaldehyde and 9-octadecyl-9H-carbazole-3-carbaldehyde. The corresponding aromatic aldehydes and 4,4'-dimethyl-2,2'-bipyridyl were reacted in a pressure tube in the presence of excess of chlorotrimethylsilane to produce the corresponding bis-stilbazole in Knoevenagel condensation type reaction[20]. The exact synthetic procedures for the ligands and complexes can be found in ESI.

The proposed Ru (II) sensitizers were then synthesized in the typical one pot three steps synthetic scheme as given in ESI. The yield of the crude products was in the range of 90-95%, which was purified through Sephadex LH-20 column for three times to get the highly pure product in 50-57% yield. The pure product was then characterized by ^{1}H-NMR, and high resolution mass spectrometry (ESI). The chemical structures of HD-14, HD-15, NCSU-10 and
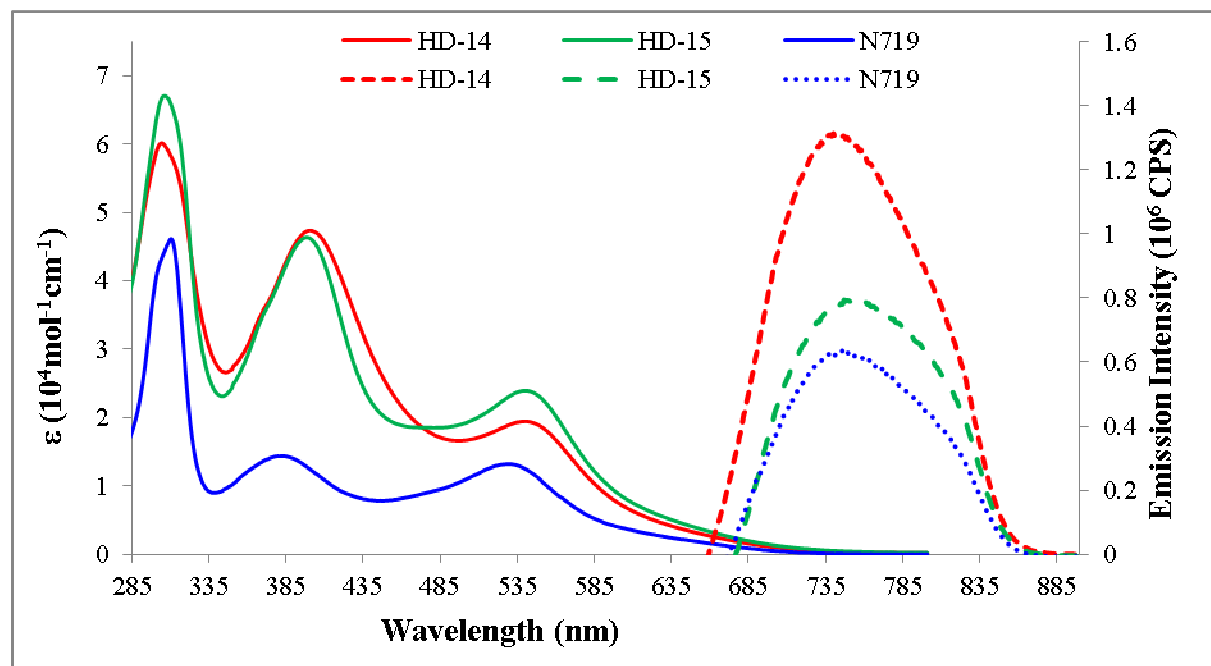
N719 are depicted in Figure 2.

TBA = n-tetrabutyl ammonium
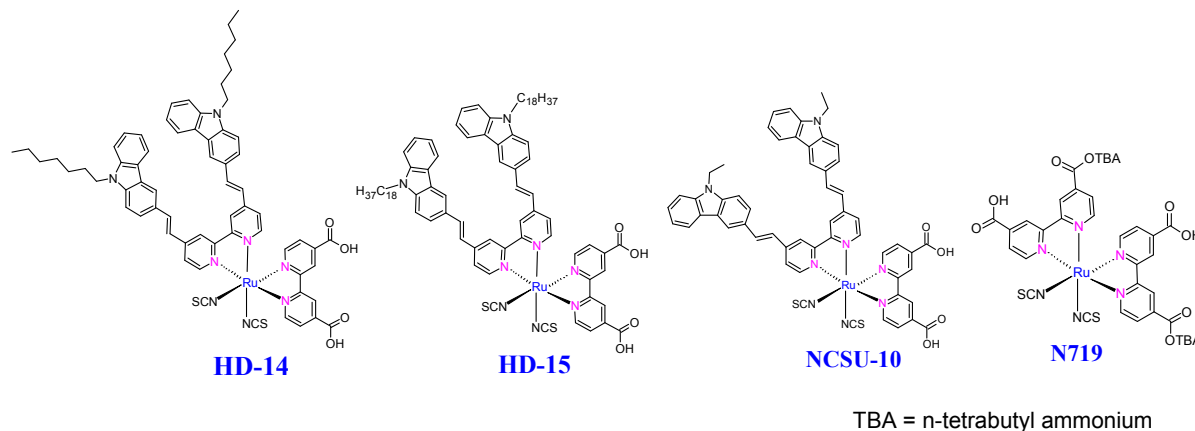
Figure 2.Molecular structures of complexes HD-14, HD-15, NCSU-10 and N719.

2.1. Photophysical Measurements

A comparison among the UV-Vis absorption and emission spectra of HD-14, HD-15 and N719, measured in DMF using concentration of 2 x10^{-5} M, is given in Figure 3 and the results are summarized in Table 1.


Figure 3. UV-Vis absorption (solid-lines) and emission spectra (dashed-lines) of complexes HD-14, and HD-15, and N719 measured in DMF (2 x10^{-5}M).

Table 1. Absorption and emission properties for HD-14, and HD-15 compared to NCSU-10 and N719.

Sensitizer	Absorption λ_{max} (nm)	ϵ (M^{-1} cm^{-1})	Emission, λ_{max} (nm)
HD-14	304,400,539(d→π*)	60,150; 47,350; 19,450	731
HD-15	306,398,539(d→π*)	67,000; 46,350; 23,950	750
NCSU-10[*]	304, 401,545 (d→π*)	57,550; 48,555; 20,650	758
N719	310,381,529(d→π*)	46 100; 14,400; 12,800	744

[*]NCSU-10 results were reported previously[19].

   Intense MLCT absorption peaks were found for HD-14, and HD-15 at 539nm with extinction coefficient of 19,450 M^{-1}cm^{-1}, 23,950M^{-1}cm^{-1}, respectively, compared to N719 at 529nm (12,800 M^{-1}cm^{-1}). The introduction of strong electron donating carbazole ancillary ligands resulted in higher molar extinction coefficient of HD-14 and HD-15 than that ofN719. Additionally, the λ_{max} of the low energy MLCT was also red shifted by up to 10nm as compared to N719. This effect can be attributed to the extended π-conjugation and stronger electron donating carbazole ligand, which resulted in destabilization of the metal-based HOMO (t_{2g}), and that translated into red shifted absorption spectra due to the decreased HOMO-LUMO gap for HD-14-15 compared to that of N719, as shown schematically in the energy level diagram of Figure 4. Additionally, incorporation of stronger ancillary ligands for HD-14 and HD-15 resulted in stronger emission than N719 as being previously reported for NCSU-10 and MH11[19, 25]. Hence, it is expected that under similar conditions and concentration, HD-14 and HD-15 are less prone to radiation-less energy losses through internal conversion and/or intersystem crossing compared to N719.
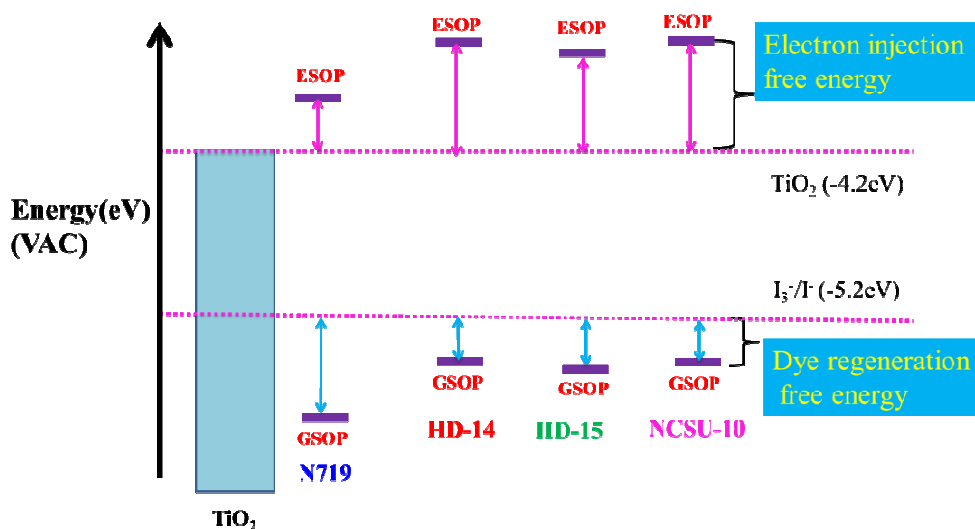
Figure 4. Energy level diagram and comparison between GSOP and ESOP of N719, HD-14, HD-15 and NCSU-10. ΔG shows the free energy of dye regeneration and electron injection

2.2. Electrochemical Measurements

The ground state oxidation potential (GSOP) of HD-14, HD-15 and NCSU-10 were measured by cyclic voltammetry (CV) in solution and the results are summarized in Table 2. CV voltammograms were used to calculate the oxidation onset which is equivalent to the GSOP (ground state oxidation potential) or HOMO level of the dye. Additionally, E_{0-0} was calculated from the onset of absorption spectrum. The values of E_{0-0} and GSOP were used to calculate the ESOP (excited state oxidation potential), the values in volts (V) against NHE were converted to electron volt (eV) by the addition of 4.7 as give in Equation 2.

$$ESOP = [(GSOP (V) +4.7) - E_{0-0}] \text{ eV} \qquad \text{Equation (2)}$$

The difference in energy of ESOP to TiO$_2$ CB has been rationalized as electron injection free energy and difference of GSOP from redox potential of I$_3^-$/I$^-$ is the dye regeneration free energy. This interrelationship between the GSOP, ESOP, electron injection and dye regeneration for HD-14, HD-15, NCSU-10 and N-719 is summarized in Figure 4. The GSOP values of -5.45 and -5.48 eV for HD-14, and HD-15, respectively confirmed that the HOMO level of these dyes are below the I$_3^-$/I$^-$ redox couple (-5.2 eV) [26], and there is enough thermodynamic driving force for

efficient dye regeneration. Additionally, ESOP of HD-14, and HD-15 were at -3.57 and -3.65eV, respectively, which lay above the conduction band edge of nanocrystalline TiO_2 (-4.2 eV) [27]. Hence, owing to energetically favorable excited states, the efficient electron injection into the CB edge of TiO_2 and dye regeneration was achieved with sensitizers HD-14, and HD-15.

Table 2. Excited state oxidation potential ($Ru^{3+/2+}$), and the lowest electronic transitions (E_{0-0}) for HD-14, HD-15, NCSU-10 and N719.

Sensitizer	Experimental (eV)		
	*E_{0-0}	♥GSOP(HOMO) (CV)	E* ($Ru^{3+/2+}$)
HD-14	1.88	-5.45	-3.57
HD-15	1.83	-5.48	-3.65
NCSU-10	1.88	-5.47	-3.59
N719	1.99	-5.76	-3.77

♥GSOP=ground state oxidation potential= E_{HOMO}; *E_{0-0}= calculated from the onset of absorption, ♥GSOP was measured in DMF with 0.1 M [TBA][PF6] and with a scan rate of 50 mV s^{-1}. It was calibrated with Fc/Fc$^+$ as internal reference and converted to NHE by addition of 0.63 V. Excited-state oxidation potential, E* ($Ru^{3+/2+}$), was calculated from: E* ($Ru^{3+/2+}$) = GSOP - *E_{0-0}. Calculated GSOP, ESOP, and E_{0-0} of N719 was performed elsewhere [28].

2.3. Photovoltaic Device Characterizations

The photovoltaic performance of complexes HD-14 and HD-15 on nanocrystalline TiO_2 electrode was studied under standard AM 1.5 irradiation (100 mW cm^{-2}) one sun illumination using an electrolyte with the composition of 0.6 M dimethylpropyl-imidazolium iodide (DMPII), 0.05 M I_2, 0.1 M LiI in acetonitrile. Figure 5 shows the incident-photon-to-current conversion efficiency (IPCE) spectra for the cells fabricated with complexes HD-14, HD-15, NCSU-10 and N719, where the incident photon-to-current conversion efficiency (IPCE) values are plotted as a function of wavelength. NCSU-10 results were reported previously [19].
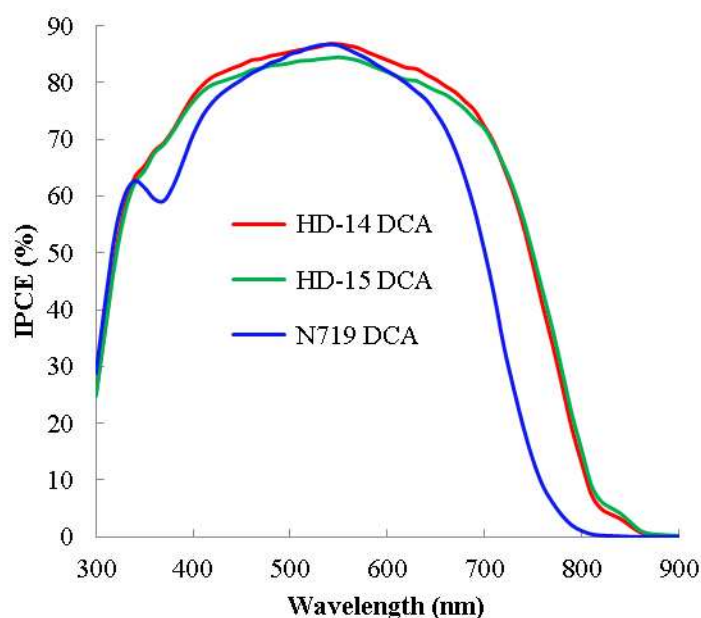
Figure 5. Photocurrent action spectra (IPCE) obtained with dyes HD-14, HD-15, and N719 anchored on nanocrystalline TiO_2 film (Electrolyte contains no TBP, DCA 20mM).

The strong photon harvesting features of carbazole ancillary ligand translated into impressive quantum efficiency for HD-14 and HD-15. Up to 80% of quantum efficiency was achieved in the plateau region. Higher molar extinction coefficient of HD-14 and HD-15 translated into superior IPCE compared to N719 both in the visible and NIR regions which resulted into higher photocurrent density as given in I-V curve of Figure 6. IPCE curves for DSCs employing HD-14 and HD-15 prepared in the presence of 0.5M TBP and DCA 20mM are shown in Figure S15a and b, of the supplementary information.
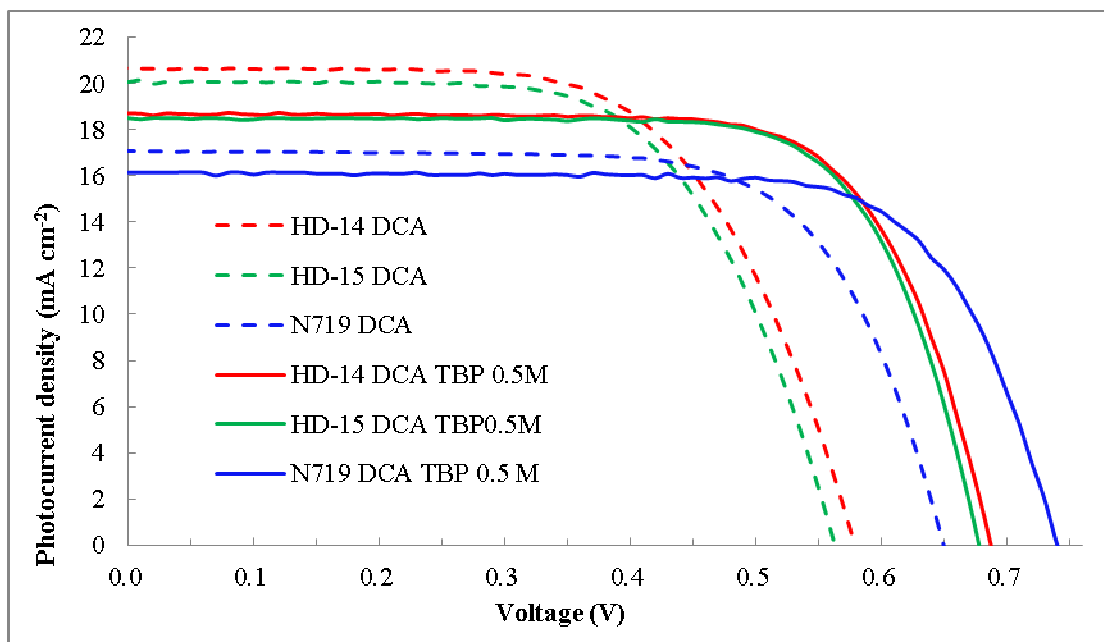
Figure 6. Photocurrent-voltage characteristics of DSCs sensitized with the complexes HD-14, HD-15 and N719 Electrolyte, 0.6 M DMPII, 0.1 M LiI, 0.05 I₂ in acetonitrile (AN), with coadsorbate DCA 20mM only (dotted line), and DCA 20mM and TBP 0.5M (solid line).

The photovoltaic parameters including the short-circuit photocurrent density (J_{sc}), open-circuit voltage (V_{oc}), fill factors (ff) and overall cell efficiencies (η) are summarized in Table 3. HD-14 and HD-15 showed impressively higher photocurrent density compared to N719 due to extended conjugation, strong electron donating carbazole ancillary ligands, and thermodynamically more favorable ground and excited state properties. I-V results for NCSU-10 were reported previously where *El-Shafei et al* [19] recognized the carbazole-based ancillary ligand with ethyl group tethered to N-carbazole being highly efficient for DSC's. By comparing the photocurrent of NCSU-10 (C2), HD-14(C7) and HD-15 (C18), it can be seen that the presence of alkyl chains of different lengths does not considerably affect the photon harvesting efficiency of the carbazole-based ancillary ligands. However, a drop in the V_{oc} of HD-14 and HD-15 compared to NCSU-10 was observed, which can be attributed to the repellent effect of the long alkyl chain between the HOMO of the dye and electrolyte, which could hinder the dye regeneration. Furthermore, no improvement in the V_{oc} for HD-14 and HD-15 was observed despite the large spacing between

TiO$_2$ and electrolyte created by the hydrophobic nature of long alkyl chains, nevertheless improvement in long term stability was anticipated. HD-14 (C7) and HD-15 (C18) showed similar V_{oc}, which contradicts previous report of collapsed C18 [29].

In order to determine the best working conditions for HD-14 and HD-15, a systematic study was designed to study the effect of TBP (tert-butylpyridine) and DCA (deoxycholic acid). TBP is well known for its effect on suppressing the recombinations of injected electrons with I$_3^-$ in electrolyte. TBP causes a negative increase in the conduction band edge of TiO$_2$, due to its basicity [30-32]. Similarly DCA as a coadsorber can be added to the dye solution upon dye adsorption to achieve TiO$_2$ surface passivation in order to suppress the recombination reactions (dark current). Coadsorbers are believed to assist in favorable packing of the dye by covering the spaces between dye molecules. However, coadsorbers have been reported to decrease the dye loading up to 60% [33] which can significantly lower the photocurrent density, such a decrease in dye loading in the presence of DCA (20mM) was not observed for HD-14 and HD-15 based on the IPCE response as given in Figure S15.

The effect of TBP and DCA alone and in combination on photovoltaic characteristics of HD-14 and HD-15 is summarized in Table 3 and shown in SI Figures S15 and S16 for IPCE and I-V results.

Table 3. Photovoltaic characteristics of HD-14, HD-15, NCSU-10 and N719.

Sensitizer	DCA (mM)	TBP (M)	J_{sc}(mA cm^{-2})	V_{oc} (V)	FF	η (%)
HD-14	0.0	0.0	20.62	0.586	0.663	8.02
	0.0	0.5	18.55	0.683	0.725	9.20
	20.0	0.0	20.66	0.579	0.629	7.51
	20.0	**0.5**	**18.71**	**0.687**	**0.721**	**9.27**
HD-15	0.0	0.0	20.88	0.557	0.625	7.27
	0.0	0.5	18.52	0.670	0.728	9.04
	20.0	0.0	20.07	0.563	0.641	7.24
	20.0	**0.5**	**18.50**	**0.679**	**0.731**	**9.17**
NCSU-10▲	20.0	0.5	19.58	0.713	0.730	**10.19**
N719	20.0	0.0	17.07	0.648	0.695	7.70

	20.0	0.5	16.15	0.745	0.741	8.92

[a]Conditions: sealed cells; photoelectrode, TiO_2 (15 μm thickness and 0.25 cm^2); electrolyte, 0.6 M DMPII, 0.1 M LiI, 0.05 I_2 in AN; irradiated light, AM 1.5 solar light (100 mW cm^{-2}). J_{sc}, short-circuit photocurrent density; V_{oc}, open-circuit photovoltage; FF, fill factor; η, total power conversion, all the results are the average of two cells. ▲NCSU-10 results were reported previously[19].

The effect of TBP alone is more prominent on HD-15 as compared to HD-14, in decreasing J_{sc}. Since LUMO of HD-15 is at -3.65eV compared to -3.57eV (more free energy) for HD-14 (Figure 4), the drop in J_{sc} of HD-15 following addition of TBA, is due to the small electron injection free energy of HD-15 compared to that of HD-14. On the contrary, J_{sc} of HD-14 increased by 0.04 mA/cm^2 on the addition of DCA and that of HD-15 decreases by 0.81 mA/cm^2. Similarly, the presence of both TBP (0.5M) and DCA (20mM) in dye solution during the adsorption onto TiO_2, resulted in increase in the V_{oc} from 0.586V to 0.687V for HD-14, with considerable increase in η% from 8.02 to 9.27. For HD-15, V_{oc} increased from 0.557V to 0.679V, with increased η% from 7.27 to 9.17. Comparatively, greater change was observed in J_{sc} as compared to V_{oc} in the presence of both TBP and DCA. For HD-14, it decreased from 20.62 mA/cm^2 to 18.71 mA/cm^2 with total decrease of 1.91 mA/cm^2. Under similar conditions, the total decrease was 2.38 mA/cm^2 for HD-15 from 20.88 mA/cm^2 to 18.50 mA/cm^2. The reasons for this decrease are the same as discussed above.

## 2.4. Electrochemical Impedance Spectroscopy Characterization

EIS is a powerful tool for charectrizing the interfacial charge transfer process at TiO_2/electrolyte and pt/electrolyte in DSCs. Combination of charge tranfer resistance and chemical capacitance give rise to a semi cirle at the complex plan. In a typical EIS experiment, the first semicircle at high frequecy corresponds to the cathode in a DSC, the middle semicircle corresponds to charge transfer resistance at the interface of dye/TiO_2 combined with chemical capacitance of electrons in TiO_2 (eTiO_2), and the third semicircle corresponds to finite Warburg

impedance element [34]. In Nyquist plot (Figure 7), the middle frequecy semicirles were in the following order of increased charge recombinations resistance N719>NCSU-10>HD-14>HD-15, which was in the order of the actual photovoltage obtained from the corresponding solar devices. Thus, the higher the charge recombination resistance in Nyquist plot, the higher the photovoltage obtained from solar cells will be owing to slower charge recobination of electrons in TiO_2 (eTiO_2) and electron acceptors in electrolyte, resulting in higher eTiO_2 lifetime[35-37].

In Figure 8, the frequency response in the range of 1-100 Hz indicates the recombination of eTiO_2 with electrolyte as the function of eTiO_2 lifetime. The injected electron lifetime eTiO_2 can be detremined by using the relation (τ_{CB}= 1/(2πf), where τ is the lifetime of electrons in TiO_2 and f is the mid-frequency peak in Bode plots. eTiO_2 depends on the density of charge traps, which is ultimately related to V_{oc}. In other words, the Bode plot results complement the Nyquist plot. The frequency peak of the DSCs in the range of 1-100 Hz based on HD-14, HD-15, NCSU-10 and N719 were at 35Hz, 35Hz, 31Hz and 20Hz, corresponding to eTiO_2 of 4.5ms, 4.5ms, 5.0ms and 8 ms, respectively, thus resulting in lower V_{oc} for HD-14 and HD-15 compared to N719 and NCSU-10, which correlates well with the actual V_{oc} reported for the solar cells (Table 3). A similar trend was also observed in the Nyquist plots (Figure 7).
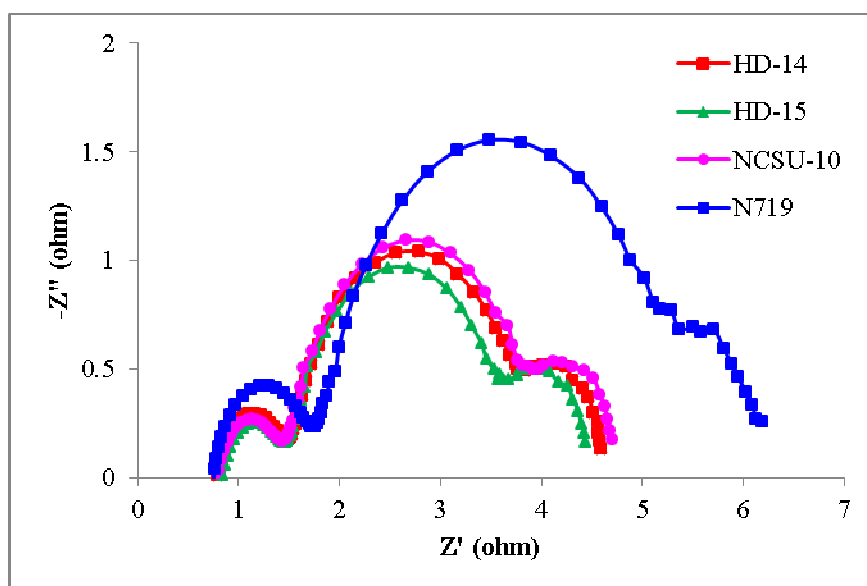
Figure 7. EIS Nyquist plots for DSCs sensitized with HD-14, HD-15, N719 and NCSU-10.
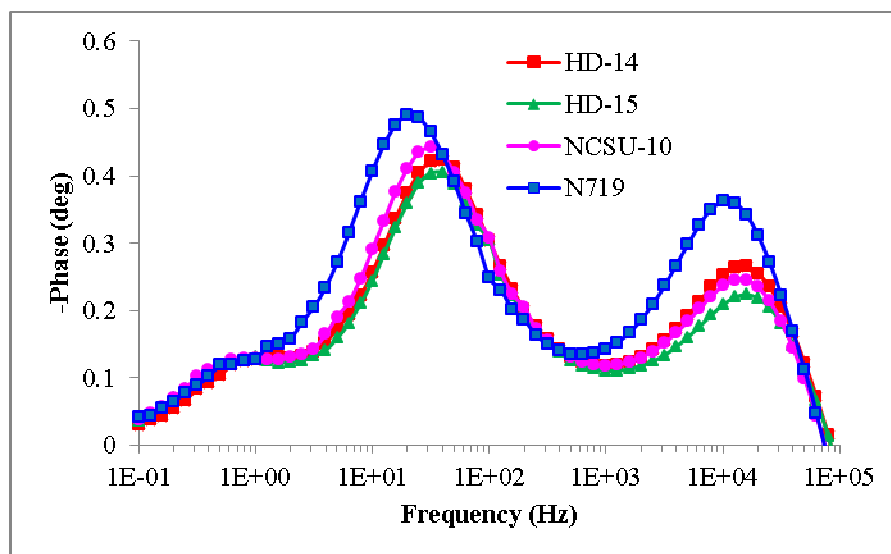
Figure 8. EIS Bode plots for DSCs sensitized with HD-14, HD-15, N719 and NCSU-10.

Long alkyl chain can suppress the dye aggregation on the TiO_2 film during dye uptake process and improve the device efficiency. Such an improvement is mainly observed in the planer structure e.g., organic dyes. In case of Ru-based (octahedral) small size dyes, like N719, dye aggregation is not so strong and a compact monolayer on the TiO_2 film can form easily, resulting in a long electron lifetime. One possible reason for the short lifetime in HD-14 and HD-15 based DSC can be attributed to the bulkiness of the dye molecule, thus hindering the diffusion of the dye into the narrow pores of meso-porous TiO_2 film leading to incomplete monolayer formation, which increases the recombination of conduction band electrons back to the electrolyte.

2.5. Long-term Stability Testing

Prolonged exposure of solar cells to light is inevitable, thus in order for DSCs to be practically viable, long term stability to irradiation is a must have feature. Usually DSCs are declared to pass such a stability test if it retains up to 90% of its initial values after the test[38-41]. The long term

stability of a DSC greatly depends on the sensitizer, type of electrolyte and the sealing method. Over an extended period of time, several kinds of mechanisms can lead to degradation of solar cells, such mechanisms have been discussed in detail somewhere else [41-44]. According to Grätzel[42], for a sensitizer to be stable for 20 years, it should be stable for one hundred million turnovers. Sensitizer Z-907[13] is widely known for its long term stability owing to the incorporation of long hydrophobic alkyl chains.

   In long term stability test, 1-methylbenzimidazole (MBI) was used instead of 4-terbutyl pyridine, since the latter has been identified to increase the rate of replacement reactions of NCS[45, 46], whereas 3-methodxypropionitrile (MPN) has been found to be stable with N719 and Z-907 for such long term stability tests as a solvent[47]. Thus, by minimizing the catalytic factors for sensitizer degradation, intrinsic stability of the complexes to irradiation can be estimated.
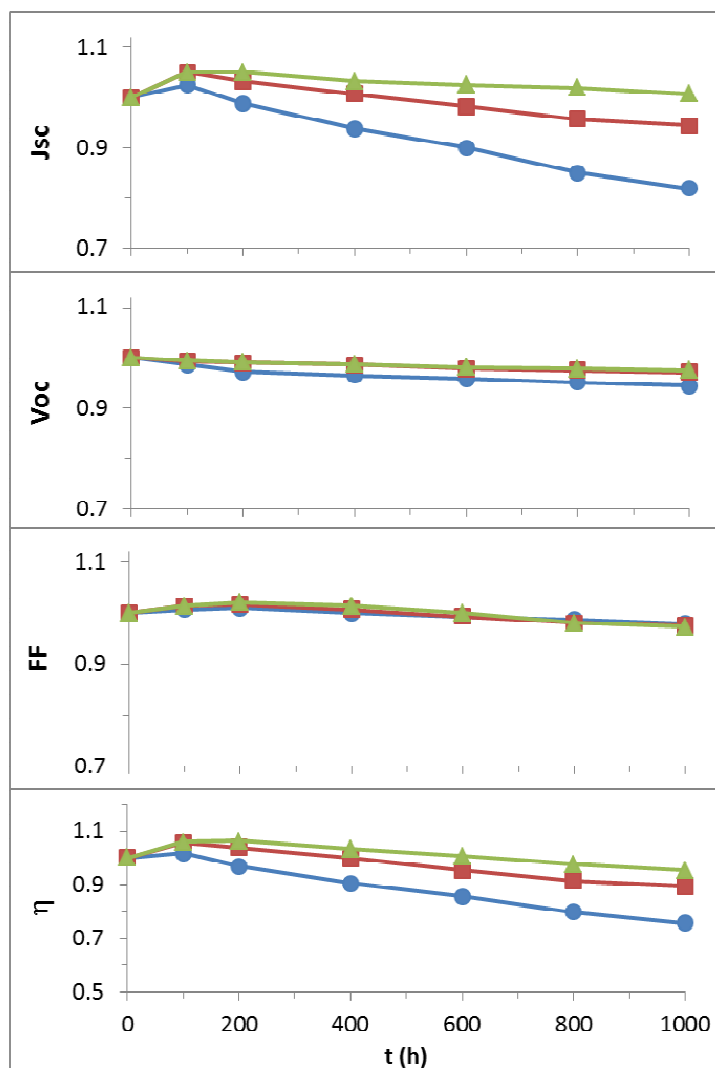
Figure 9. Evolutions of photovoltaic performance parameters for HD-14 (squares), HD-15 (triangles), and NCSU-10 (circle) based DSCs during light soaking under AM 1.5 illumination (light intensity: 100 mW cm^{-2}) over a period of 1000 h. A 420-nm cut-off filter was applied during illumination. Ionic-liquid electrolyte: 0.15 M I$_2$, 0.1 M GuSCN, 0.5 M MBI, and 1 M PMII in MPN at 25 $^{\circ}$C.

Long term stability test of HD-14, HD-15, and NCSU-10 based DSCs was carried out under 1 sun light soaking condition with 420nm cut-off filter for 1000h and the normalized results are shown in Figure 9. At time zero, HD-14 based solar device with ionic liquid electrolyte resulted in J_{sc} of 16.1 mA/cm^2; V_{oc}, 0.69V; FF, 0.72; and η of 7.9%. A slight increase in J_{sc} and η of the devices was observed after one week, which can be attributed [13] to self-assembly of long alkyl chains or more efficient dye regeneration due to the penetration of the electrolyte to the hidden

cavities for HD-15 and HD-14, whereas such a change was marginal in case of NCSU-10.

The device based on HD-15 (C18) outperformed HD-14 (C7) and NCSU-10 (C2) in terms of photostability. HD-15 was extraordinarily stable in J_{sc} as it maintained up to 100% of its initial value, compared to 4-5% loss in J_{sc} for HD-14 and up to 20% loss in J_{sc} for NCSU-10. HD-15 and HD-14 maintained V_{oc} up to 98% of initial value with slightly more loss in V_{oc} for NCSU-10. Loss in FF was less than 3% for all the sensitizers. HD-15 maintained 98% of initial conversion efficiency value compared to 92% of HD-14and 78% of NCSU-10. Thus the long alkyl chains keep the sensitizer intact even after 1000h light soaking. We attribute the stabilizing effect of long alkyl chains to the formation of compact molecular monolayer on TiO_2 surface which prevents desorption of the dye. Similarly this monolayer also prevents water and other impurities to influence the operation of DSC at TiO_2 surface.

2.6. Nanosecond Laser Flash Photolysis and Femtosecond Transient Absorption Spectroscopy

Nanosecond laser flash photolysis spectroscopy was employed to study the dye regeneration. In this experiment, we studied the decay of transient absorption spectra for HD-14, HD-15 and N719 dye-sensitized TiO_2 and the results are shown in Figure 10 (a) without electrolyte and 10 (b) with electrolyte. In the absence of an electrolyte, the decay of the absorption signal reflects the dynamics of recombination of injected electrons with the oxidized dye. The decay profiles were fitted by a stretched exponential and the recombination time for injected electrons was found to be 11.3, 9.1 and 6.9 μs for N719, HD-14 and HD-15, respectively. Moser and Grätzel[48] have reported that recombination kinetics between TiO_2 injected electrons and the oxidative dye are therefore expected to lie in the Marcus inverted region (that dictates the back electron transfer in organic photovoltaic devices) where electron transfer is thermally activated and an

increase in driving force should lead to a decrease in the transfer rate constant. Here, we showed that rising recombination kinetics rates 11.3, 9.1 and 6.9 μs for N719, HD-14 and HD-15, respectively were not exactly affected by differences in driving force (see Fig.4) as N719 has lower driving force but still lower recombination kinetic rate.

In a separate investigation, Meyer et al[49] showed that the driving forces for similar types of dyes hardly affect the recombination kinetics, and it was proposed that the kinetics were determined by diffusion-limited encounters between electrons in TiO_2 and oxidized dye molecules.
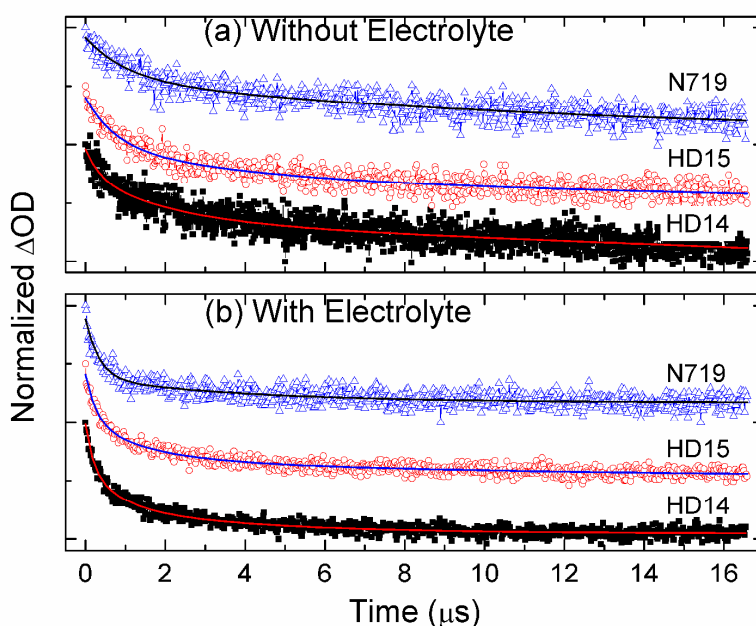

Figure 10. Transient decay profiles of HD-14, HD-15, and N719 while anchored to TiO_2 (a) without electrolyte and (b) with electrolyte.

In the presence of an electrolyte, the decay profile represents the dye regeneration through the oxidation of I^-. The fitting of the decay profiles observed for the transient absorption signal in the presence of electrolyte resulted in regeneration time equal to 2.6, 3.6, and 3.7 μs for HD-14, HD-15, and N719 dyes, respectively. Kinetically, dye regeneration is faster than recombination of injected electrons with oxidized dye (without electrolyte) if we ignore the effect of electrolyte on the recombination of injected electrons to oxidized dye. The rate for dye regeneration (HD-

14>HD-15>N719) was found to be in the same order of photocurrent density generated from devices employing HD-14, HD-15 and N719 as was reported previously[50] for Ru (II) sensitizers.

To understand how the alkyl chain length on the carbazole ligand affects the charge injection, femtosecond transient absorption spectroscopy (TAS) was performed on HD-14 and HD-15 and the results were compared with the benchmark dye N719 under similar experimental conditions. TAS graphs for HD-14, HD-15 and N719 are shown in Figure 11-12. The spectra for all three dyes (Figure 11) show ground state bleaching (GSB) spectral features at wavelength less than 600 nm (> 2 eV), which has increased transmission, as well as a photo-induced absorption (PIA) band greater than 600 nm, which has decreased transmission. The PIA band is responsive to the charge separation dynamics as it probes the oxidized dye (dye$^+$), excited state dye (dye*), and the injected electrons in the conduction band of the TiO$_2$ (eTiO$_2$), as reported previously [51-58].
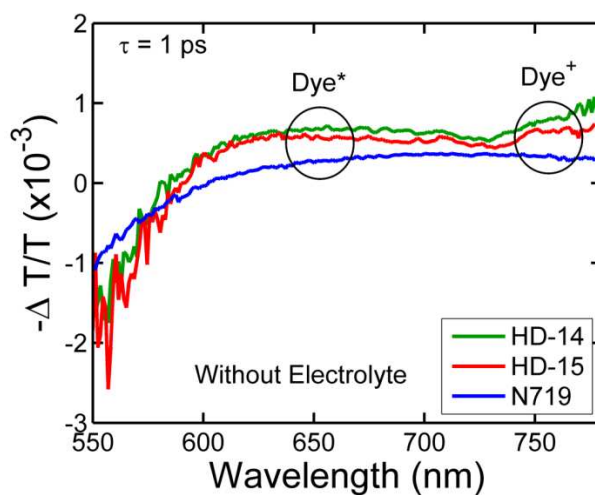

Figure 11. Transient absorption spectra at $\tau = 1$ ps of HD-14, HD-15, and N719 without the addition of the electrolyte.

Figure 12, shows the transient absorption signal for HD-14 and HD-15 individually with delay times of 0ps and 500 ps and it clearly shows the absorption features of GSB (<600nm) and PIA for dye* (660nm) and dye$^+$ (760) similar to Figure 11.
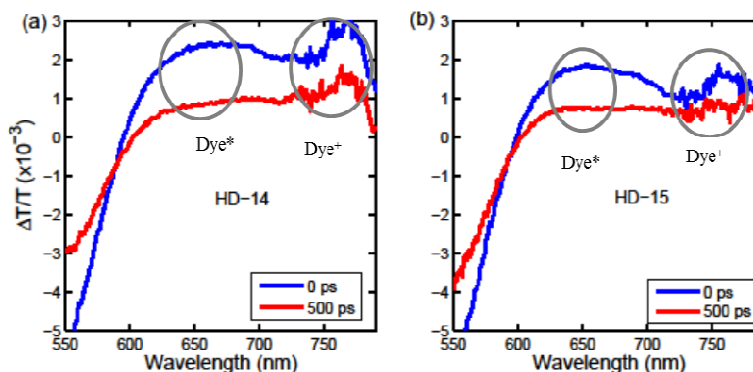
Figure 12. Transient absorption spectra at $\tau = 0$ ps and $\tau = 500$ ps of HD-14 (a) and HD-15 (b) with the electrolyte.

We compared the charge injection by monitoring the amplitude of the TA signal at 760 nm which corresponds to the absorption for oxidized dye (dye$^+$) after excitation at 530 nm. Figure 13 shows the oxidized dye (dye$^+$) dynamics of the three samples in the TiO$_2$/dye/electrolyte DSC structure. The dynamics of the three samples without the electrolyte are given in Figure S18. In Figure 13, the comparison of the kinetics at 760 nm between the three dyes clearly shows a difference in charge injection. The dynamics in all three DSC structures exhibit a sharp, fast component (<1ps) due to singlet injection. However, N719 shows a second slow rise component which can be attributed to triplet injection, whereas HD-15 remains flat after ~ 1ps and HD-14 has a slight decay. The dynamics at 760 nm became flat after 500 ps in all three DSCs. We compared the amplitude of the TA signal after 1000 ps and found that HD-14 and HD-15 based DSCs have the signal ~1.71 and ~1.59 times higher than that of N719. On the other hand, photocurrent density obtained from cells (Table 3) for HD-14 and HD-15 is ~1.12 and ~1.10 times higher than that of N719. We found that the amplitude of the TA signal of the oxidized dye, which corresponds to the injection efficiency, correlates well with the photocurrent density and as a result to the solar cell total conversion efficiency.
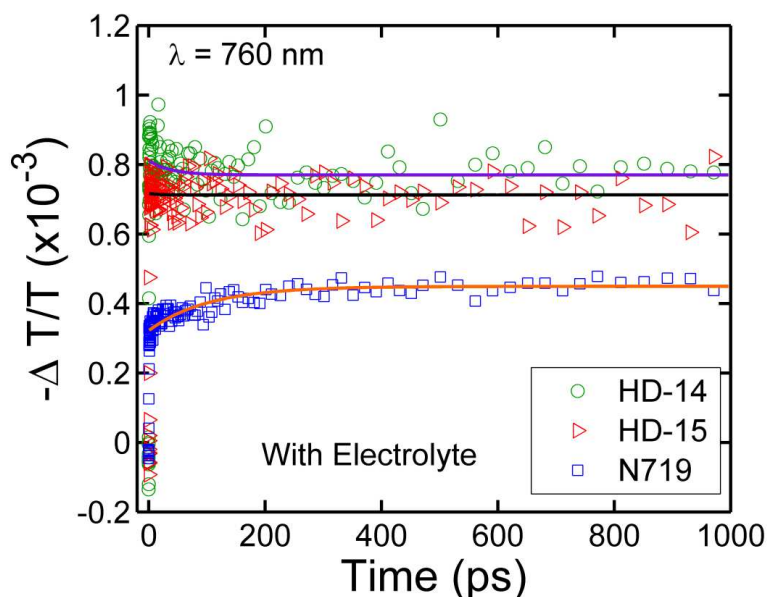
Figure 13. Transient absorption dynamics of HD-14, HD-15, and N719 at 760 nm in the presence of the electrolyte.

3. CONCLUSIONS

It can be concluded on the basis of this study that carbazole-based ancillary ligands has a great potential to be employed with simple molecular design strategy based on different alkyl chain lengths to enhance the long term stability and photon harvesting efficiency of the sensitizers, which ultimately translates into higher molar extinction coefficient and overall greater photocurrent response of the solar device. Cyclic voltammetry results showed that the novel sensitizers HD-14 and HD-15 offer more thermodynamic free energy for electron injection into TiO_2 as compared to N719. This fine tuning of optical and photopysical properties resulted in up to 20% higher photocurrent response for HD-14 and HD-15 compared to N719. Strategy of tethering long alkyl chains to N-carbazole resulted in solar-to-power conversion efficiency ($\eta\%$) of 9.27 for HD-14 and 9.17 for HD-15 against 8.92 of N719 and enhanced long term stability, under similar conditions. HD-15 showed strikingly good long term light soaking stability and maintained up to 98% of initial value compared to 92% for HD-14 and 78% for NCSU-10. Thus, it can be concluded that longer alkyl chains such as C18 in the case of HD-15 can be utilized

efficiently without hampering the electron injection and dye regeneration as shown by femto second and laser flash photolysis spectroscopy. It was found from laser flash photolysis transient absorption spectroscopy experiments for dye regeneration that the dye regeneration for HD-15 (3.6 μs) is slower than that of HD-14 (2.6 μs) likely due the spatial effect generated by C18 chains between the dye and electrolyte. Thus slightly lower V_{oc} of HD-15 compared to that of HD-14 can be rationalized on the basis of slower dye regeneration and shorter eTiO$_2$ as found by impedance measurements. This work clearly shows the benefit of having long alkyl chains in heteroleptic Ru (II) sensitizer on strong electron donor carbazole groups in terms of long term stability, paving the way for wide spread application of highly efficient and durable DSCs.

Supporting Information

Synthesis details, FT-IR, High-Resolution ESI-MS, ^{1}HNMR and cyclic voltammetry graphs are given as Supporting Information.

Corresponding Author Ahmed El-Shafei, Ahmed_El-Shafei@ncsu.edu

REFERENCES

1 N. S. Lewis, *Science,* 2007, **315,** 798-801.

2 M. K. Nazeeruddin, S. M. Zakeeruddin, R. Humphry-Baker, M. Jirousek, P. Liska, N. Vlachopoulos, V. Shklover, C. Fischer and M. Grätzel, *Inorg. Chem.,* 1999, **38,** 6298-6305.

3 C. Grätzel and S. M. Zakeeruddin, *Materials Today,* 2013, **16,** 11-18.

4 P. Péchy, T. Renouard, S. M. Zakeeruddin, R. Humphry-Baker, P. Comte, P. Liska, L. Cevey, E. Costa, V. Shklover, L. Spiccia, G. B. Deacon, C. A. Bignozzi and M. Grätzel, *J. Am. Chem. Soc.,* 2001, **123,** 1613-1624.

5 S. Zhang, X. Yang, Y. Numata and L. Han, *Energy Environ. Sci.,* 2013, **6,** 1443-1464.

6 B. O'Regan and M. Grätzel, *Nature,* 1991, **353,** 737-740.

7 S. Mathew, A. Yella, P. Gao, R. Humphry-Baker, F. E. CurchodBasile, N. Ashari-Astani, I. Tavernelli, U. Rothlisberger, NazeeruddinMd. Khaja and M. Grätzel, *Nat Chem,* 2014, **6,** 242-247.

8 K. Wojciechowski, M. Saliba, T. Leijtens, A. Abate and H. J. Snaith, *Energy Environ. Sci.,* 2014, **7,** 1142-1147.

9 The National Renewable Energy Laboratory (NREL), **2014,** http://www.nrel.gov/ncpv/images/efficiency_chart.jpg

10 H. Zhou, Q. Chen, G. Li, S. Luo, T. Song, H. Duan, Z. Hong, J. You, Y. Liu and Y. Yang, *Science,* 2014, **345,** 542-546.

11 S. M. Feldt, E. A. Gibson, E. Gabrielsson, L. Sun, G. Boschloo and A. Hagfeldt, *J. Am. Chem. Soc.,* 2010, **132,** 16714-16724.

12 P. Gao, Y. J. Kim, J. Yum, T. W. Holcombe, M. K. Nazeeruddin and M. Grätzel, *J. Mater. Chem. A,* 2013, **1,** 5535-5544.

13 P. Wang, S. M. Zakeeruddin, J. E. Moser, M. K. Nazeeruddin, T. Sekiguchi and M. Grätzel, *Nat Mater,* 2003, **2,** 402-407.

14 D. Shi, N. Pootrakulchote, R. Li, J. Guo, Y. Wang, S. M. Zakeeruddin, M. Grätzel and P. Wang, *J. Phys. Chem. C,* 2008, **112,** 17046-17050.

15 F. Gao, Y. Wang, J. Zhang, D. Shi, M. Wang, R. Humphry-Baker, P. Wang, S. M. Zakeeruddin and M. Grätzel, *Chem. Commun.,* 2008, 2635-2637.

16 C. Chen, J. Chen, S. Wu, J. Li, C. Wu and K. Ho, *Angewandte Chemie International Edition,* 2008, **47,** 7342-7345.

17 S. Fan, C. Kim, B. Fang, K. Liao, G. Yang, C. Li, J. Kim and J. Ko, *J. Phys. Chem. C,* 2011, **115,** 7747-7754.

18 C. Chen, N. Pootrakulchote, S. Wu, M. Wang, J. Li, J. Tsai, C. Wu, S. M. Zakeeruddin and M. Grätzel, *J. Phys. Chem. C,* 2009, **113,** 20752-20757.

19 A. El-Shafei, M. Hussain, A. Atiq, A. Islam and L. Han, *J. Mater. Chem.,* 2012, **22,** 24048-24056.

20 A. El-Shafei, M. Hussain, A. Islam and L. Han, *J. Mater. Chem. A,* 2013, **1,** 13679-13686.

21 H. Cheema, A. Islam, L. Han and A. El-Shafei, ACS Appl. Mater. Interfaces, 2014, 6, 11617-11624.

22 H. Cheema, A. Islam, L. Han, B. Gautam, R. Younts, K. Gundogdu and A. El-Shafei, J. Mater. Chem. A, 2014, 2, 14228-14235.

23 Z. Zhang, M. Fujiki, H. Tang, M. Motonaga and K. Torimitsu, *Macromolecules,* 2002, **35,** 1988-1990.

24 Y. Zhan, K. Cao, C. Wang, J. Jia, P. Xue, X. Liu, X. Duan and R. Lu, *Org. Biomol. Chem.,* 2012, **10,** 8701-8709.

25 M. Hussain, A. El-Shafei, A. Islam and L. Han, *Phys. Chem. Chem. Phys.,* 2013, **15,** 8401-8408.

26 G. Oskam, B. V. Bergeron, G. J. Meyer and P. C. Searson, *J Phys Chem B,* 2001, **105,** 6867-6873.

27 A. Hagfeldt and M. Grätzel, *Chem. Rev.,* 1995, **95,** 49-68.

28 M. K. Nazeeruddin, F. De Angelis, S. Fantacci, A. Selloni, G. Viscardi, P. Liska, S. Ito, B. Takeru and M. Grätzel, *J. Am. Chem. Soc.,* 2005, **127,** 16835-16847.

29 L. Schmidt-Mende, J. E. Kroeze, J. R. Durrant, M. K. Nazeeruddin and M. Grätzel, *Nano Lett.,* 2005, **5,** 1315-1320.

30 K. Hara, Y. Dan-oh, C. Kasada, Y. Ohga, A. Shinpo, S. Suga, K. Sayama and H. Arakawa, *Langmuir,* 2004, **20,** 4205-4210.

31 G. Schlichthorl, S. Y. Huang, J. Sprague and A. J. Frank, *J Phys Chem B,* 1997, **101,** 8141-8155.

32 S. A. Haque, Y. Tachibana, R. L. Willis, J. E. Moser, M. Grätzel, D. R. Klug and J. R. Durrant, *J Phys Chem B,* 2000, **104,** 538-547.

33 N. R. Neale, N. Kopidakis, d. L. van, M. Grätzel and A. J. Frank, *J Phys Chem B,* 2005, **109,** 23183-23189.

34 Kalyanasundaram, K., *Dye-Sensitized Solar Cells,* CRC ; Taylor & Francis, Boca Raton, Fla.; London, 2009.

35 F. Fabregat-Santiago, J. Bisquert, G. Garcia-Belmonte, G. Boschloo and A. Hagfeldt, *Solar Energy Mater. Solar Cells,* 2005, **87,** 117-131.

36 M. S. Gaes, E. Joanni, E. C. Muniz, R. Savu, T. R. Habeck, P. R. Bueno and F. Fabregat-Santiago, *J. Phys. Chem. C,* 2012, **116,** 12415-12421.

37 K. Wu, W. Ku, J. N. Clifford, E. Palomares, S. Ho, Y. Chi, S. Liu, P. Chou, M. K. Nazeeruddin and M. Grätzel, *Energy Environ. Sci.,* 2013, **6,** 859-870.

38 D. Kuang, C. Klein, S. Ito, J. Moser, R. Humphry-Baker, N. Evans, F. Duriaux, C. Grätzel, S. . Zakeeruddin and M. Grätzel, *Adv Mater,* 2007, **19,** 1133-1137.

39 P. Wang, C. Klein, R. Humphry-Baker, S. M. Zakeeruddin and M. Grätzel, *J. Am. Chem. Soc.,* 2005, **127,** 808-809.

40 P. Wang, S. M. Zakeeruddin, J. E. Moser, M. K. Nazeeruddin, T. Sekiguchi and M. Grätzel, *Nat Mater,* 2003, **2,** 402-407.

41 M. I. Asghar, K. Miettunen, J. Halme, P. Vahermaa, M. Toivola, K. Aitola and P. Lund, *Energy Environ. Sci.,* 2010, **3,** 418-426.

42 M. Grätzel, *Comptes Rendus Chimie,* 2006, **9,** 578-583.

43 R. Harikisun and H. Desilvestro, *Solar Energy,* 2011, **85,** 1179-1188.

44 P. M. Sommeling, M. Späth, H. J. P. Smit, N. J. Bakker and J. M. Kroon, *J. Photochem. Photobiol. A.,* 2004, **164,** 137-144.

45 H. T. Nguyen, H. M. Ta and T. Lund, *Solar Energy Mater. Solar Cells,* 2007, **91,** 1934-1942.

46 P. Tuyet Nguyen, R. Degn, H. Thai Nguyen and T. Lund, *Solar Energy Mater. Solar Cells,* 2009, **93,** 1939-1945.

47 D. Kuang, S. Ito, B. Wenger, C. Klein, J. Moser, R. Humphry-Baker, S. M. Zakeeruddin and M. Grätzel, *J. Am. Chem. Soc.,* 2006, **128,** 4146-4154.

48 J. E. Moser and M. Grätzel, *Chem. Phys.,* 1993, **176,** 493-500.

49 C. A. Kelly, F. Farzad, D. W. Thompson, J. M. Stipkala and G. J. Meyer, *Langmuir,* 1999, **15,** 7047-7054.

50 M. Hussain, A. Islam, I. Bedja, R. K. Gupta, L. Han and A. El-Shafei, *Phys. Chem. Chem. Phys.,* 2014, **16**, 14874-14881.

51 G. Benko, J. Kallioinen, J. Korppi-Tommola, A. P. Yartsev and V. Sundstrom, *J. Am. Chem. Soc.,* 2002, **124,** 489-493.

52 A. Furube, Z. Wang, K. Sunahara, K. Hara, R. Katoh and M. Tachiya, *J. Am. Chem. Soc.,* 2010, **132,** 6614-6615.

53 S. A. Haque, E. Palomares, B. M. Cho, A. N. M. Green, N. Hirata, D. R. Klug and J. R. Durrant, *J. Am. Chem. Soc.,* 2005, **127,** 3456-3462.

54 R. Katoh, A. Furube, M. Kasuya, N. Fuke, N. Koide and L. Han, *J. Mater. Chem.,* 2007, **17,** 3190-3196.

55 S. E. Koops, B. C. O' Regan, P. R. F. Barnes and J. R. Durrant, *J. Am. Chem. Soc.,* 2009, **131,** 4808-4818.

56 J. Sobus, G. Burdziaski, J. Karolczak, J. Idogoras, J. A. Anta and M. Ziolek *Langmuir,* 2014, **30,** 2505-2512.

57 Y. Tachibana, J. E. Moser, M. Grätzel, D. R. Klug and J. R. Durrant, *J. Phys. Chem.,* 1996, **100,** 20056-20062.

58 J. Teuscher, J. Dacoppet, A. Punzi, S. M. Zakeeruddin, J. Moser and M. Gr¨atzel, J. Phys.

Chem. Lett., 2012, 3, 3786–3790.